Plastic Deformation of Amorphous Poly(L/DL-lactide): Structure Evolution and Physical Properties

Miroslaw Pluta* and Andrzej Galeski

Centre of Molecular and Macromolecular Studies, Polish Academy of Sciences, Sienkiewicza 112, 90-363 Lodz, Poland

Received December 27, 2006; Revised Manuscript Received March 12, 2007

Plastic deformation of amorphous, thermally noncrystallizable poly(L/DL-lactide) 70/30 (P(L/DL)LA) was induced by a plane-strain compression in a channel-die at different temperatures, above the glass transition (T_g) from 60 to 90 °C. Samples undeformed (reference) and deformed to different compression ratios, from 4.6 to 23.0, were studied by X-ray diffraction, thermally modulated differential scanning calorimetry, light microscopy, and mechanical methods—viscoelastic and tensile tests. The effects of the compression ratios and deformation temperatures on the final structure and properties of the P(L/DL)LA were evaluated. It was revealed that plastic deformation transformed an amorphous P(L/DL)LA (thermally noncrystallizable) to a crystalline fibrillar texture oriented in the flow direction. Fibrillar texture was formed in spite of the tendency of the plane-strain compression to form single-crystal-like texture. The crystallite size in the transverse direction was small, up to 90 Å at the highest compression ratio. No evidence of lamellar organization and features of supermolecular structure were detected by small-angle X-ray scattering and light microscopy, respectively. The oriented samples exhibited a low crystallinity degree at the level of 6−9% at the highest compression ratio. The main transformation mechanism was shear and orientation-induced crystallization. The crystalline phase was in the α crystallographic modification of poly(lactide) typically formed in more stereoregular poly(lactide) by thermal treatment. The glass transition increased with the increase of compression ratio reflecting the increase of orientation of the polymer chains. The tensile strength of deformed samples was improved considerably in comparison to that of the reference sample.

Introduction

Poly(lactide) is a thermoplastic polyester produced either by the ring-opening polymerization or polycondensation of lactides or lactid acid monomers, which are obtained on the basis of renewable starch-containing resources (e.g., corn, wheat, or sugar beats) by fermentation or by chemical synthesis of nonrenewable resources.[1] Poly(lactide) is a degradable and biocompatible polymer and finds various commercial applications in the production of disposable items (compost bags, plant pots, diapers, and packaging)[2] and fibers[3] in addition to well-established medical applications such as implants for bone fixation,[4] sutures,[5] drug delivery systems,[6] etc.

One of the most interesting features of the poly(lactide) is that the monomer possesses one carbon atom with chiral asymmetry. Lactide monomer may contain identical stereocenters (L, L) or (D, D) or enantiomeric stereocenters (L, D) of varying composition. Generally, L,L-enantiomers are present in greater amounts than D,D-enantiomers. Introducing of D-mers into the L-chain disturbs its stereoregularity and lowers its ability to crystallize. When the d content is greater than 15% a fully amorphous, noncrystallizable under heat treatment, polymer is obtained.

It is known that pure poly(lactide)s can form two crystal modifications. The most common modification is the α form classified sometimes as pseudo-orthorhombic,[7,8] pseudohexagonal,[9] or orthorhombic[8,10−13] with 10_3 helix conformation of the chain. The α form is usually formed during processing of the polymer via thermal treatment or from solutions. The second crystalline modification is a β form—orthorhombic[14−17] with a 3_1 helical chain conformation. The β form is obtained via transformation of the α crystalline form during drawing of semicrystalline poly(lactide) to a large strain ratio above the glass transition (T_g). The ratio of the β to the α form increases with the temperature and degree of deformation.

Physicochemical properties of poly(lactide) are affected strongly by the crystallinity degree and the overall morphology. The physical structure can be controlled by thermal treatment and, in addition, by application of orientation processes in order to introduce preferential structural arrangement. In the case of thermally crystallizable poly(lactide) the following thermo−mechanical methods were applied for improving its properties so far: orientrusion[18] self-reinforcing method,[19] solid-state extrusion technique,[14−16,20,21] tensile drawing.[17] These methods allow one to produce oriented materials with improved mechanical properties and programmed cross-sectional profile (e.g., for fixing of fractured bones). Thinner oriented poly(lactide) materials in the form of fibers were also obtained by melt-spinning and spin-drawing processes[22−24] as well as zone-drawing operations.[25]

In this work a plastic deformation of amorphous poly(L/DL-lactide) (P(L/DL)LA)) above its T_g is studied. The polymer contains 30% of DL-units incorporated between L-units. It is known that due to a decreased stereoregularity it is thermally noncrystallizable neither during melt-cooling, heating from a solid state, nor during annealing at elevated temperatures. Similar properties exhibit racemic poly(DL-lactide) 50/50 and poly(L/D-lactides) containing more than 15% of the D-unit in the chain. This type of poly(lactide)s finds application in medicine as resorbable internal fixation devices, usually after mechanical reinforcing via plastic deformation, e.g., via solid-

* Author to whom correspondence should be addresssed. Phone: +48 (42) 6803237. Fax.: +48(42) 6847126. E-mail: mpluta@bilbo.cbmm.lodz.pl.

10.1021/bm061229v CCC: $37.00
Published on Web 05/02/2007

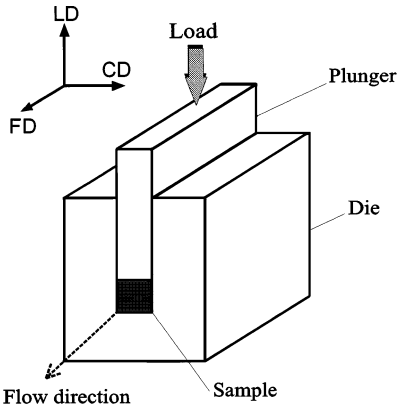

Figure 1. Diagram of compression in a channel-die.

state extrusion.[20] Without mechanical reinforcing, copolymers exhibit low modulus and enhanced ductility (elongation to break a few dozen percent), in contrast to optically pure poly(L-lactide), which is brittle and breaks at smaller elongation (1−3%). Here, a channel-die technique has been used for the study of orientation and plastic deformation of the P(L/DL)LA. This technique enables the deformation in a cavity-free manner due to a compressive stress component. The aim of this work is to study the structure alternation of thermally noncrystallizable poly(L/DL-lactide) and physical properties of compression-deformed samples. Especially, the attention was turned to the detection of orientation-induced crystallization often observed in pure poly(L-lactide). The deformation was carried out in a channel-die at different temperatures above the T_g. The arrangement of macromolecules was probed using X-ray techniques (two-dimensional wide-angle X-ray scattering (2D-WAXS), one-dimensional scans, and the pole figure method). Morphology was viewed by light microscopy. Thermal behavior during heating was studied using temperature-modulated differential scanning calorimetry (TMDSC). Mechanical properties were determined in the tensile mode using an Instron tensile testing machine at room temperature and dynamic mechanical deformation (DMTA) as a function of temperature at a constant deformation frequency.

Experimental Section

Materials. Poly(L/DL-lactide) 70/30 (P(L/DL)LA) grade LR708 was from CCA Purac Biochem (Gorinchem, Holland). Molar mass M_w = 226 000 and molar mass distribution M_w/M_n = 1.36 were calculated from the experimental size exclusion chromatography (SEC) traces using the Wyatt ASTRA v 4.90.07 program. The SEC measurement was performed using an Agilent 1100 series isocratic pump, degasser, autosampler thermostatic box for the columns, and a set of TSK gel columns (2XPLGel 5 μm MIXED-C) at 25 °C. A Wyatt Optilab rEX interferometric refractometer and MALLS DAWN EOS laser photometer (Wyatt Technology Corp., U.S.A.) were applied as detectors. Methylene chloride was used as the eluent at a flow rate of 0.8 mL/min^{-1}.

Sample Preparation. The raw polymer was dried at 100 °C for 4 h under reduced pressure. Afterward, it was compression molded in a 50 mm × 50 mm frame at 180 °C to obtain 4 mm thick plates. Subsequently, the mold was cooled down between aluminum blocks to room temperature. Those plates were cut into rectangular-shaped samples for the deformation study. Their height was up to 50 mm depending on the compression ratio (CR) targeted. The surface of the samples was polished using fine-grain sandpaper. The specimens were subjected to plane-strain compression in a channel-die (e.g., ref 26), shown schematically in Figure 1.

Table 1. Samples Abbreviations and the Processing Parameters

sample abbreviation	compression ratio (CR)	deformation temp (T_d, °C)
P1.0	1.0	
P1.0−100	1.0	
P3.9−60	3.92	60
P4.7−65	4.69	65
P6.0−70	6.00	70
P6.4−80	6.40	80
P7.3−90	7.33	90
P15.7−90	15.75	90
P23.5−90	23.50	90

Prior to the tests the specimen surfaces were lightly lubricated with a silicon grease to reduce friction against the plunger and the walls of the channel-die. Then, a specimen was placed inside a channel-die assembly and heated up for 30 min to a temperature desired for the deformation experiment. The Instron tensile testing machine model 1114 of the capacity of 50 kN was used as a loading frame. The deformation was performed above the T_g of PLA at different temperatures (T_d): 60, 65, 70, 80, and 90 °C. The crosshead speed was adjusted to the actual sample height in order to obtain the true strain rate V_d of 8%/min. The load and plunger displacement were recorded during the compression test. The compression was stopped after reaching a desired CR. The channel-die, still under load, was cooled down to ambient temperature by a cooling system (within 4 min). Afterward, the deformed sample was removed. Considered samples are specified in Table 1.The samples are coded using the following symbols: P (polymer), CR (compression ratio value), T_d (deformation temperature). In this table are also given the codes of the undeformed sample P(L/DL)LA: as received, P1.0, and annealed at 100 °C for 3 h, P1.0−100, for comparison.

Thermal Analysis. Thermal behavior of the samples was investigated using a thermally modulated DSC 2920 (TMDSC) from TA Instruments. Measurements were performed with a "heating only profile" at a ramp of 3 °C/min, with a modulation period of 40 s and a modulation temperature amplitude of 0.318 °C. The following events were characterized: glass−rubber transition (T_g), the stress relaxation activated above T_g, and the melting process. The crystallinity level was estimated based on the melting endotherm and the enthalpy of fusion, 93.1 J/g of 100% crystalline regions.[27]

Characterization. *X-ray Diffraction.* Although any crystallinity in the P(L/DL)LA copolymer was not expected, we performed an X-ray diffraction (XRD) study. Different XRD techniques were used for characterization of the crystalline structure of undeformed and deformed samples. The 1.5 mm thick specimens were carefully machined out from the deformed samples. Two-dimensional WAXS patterns were recorded in the plane perpendicular to the load direction (LD) and with the flow direction (FD) directed horizontally using image plates and Cu Kα radiation (generator Philips PW1830). Exposed imaging plates were analyzed with the PhosphorImager SI system (Molecular Dynamics). X-ray intensity distributions versus 2θ (from 10° to 50°) were also measured in the transmission and reflection modes-coupled $\theta/2\theta$, for selected orientations of the samples. A wide-angle goniometer coupled to a sealed-tube source of filtered Cu Kα radiation (Philips PW3830) was used. The same device was applied to the measurements of pole figures according to the procedure described in ref 26. The slit system of the diffractometer was adjusted to measure the integral intensity of a given diffraction peak. For the pole figure construction for the selected sample several crystallographic diffraction reflections of PLA at 2θ of 16.8° (200), 19.2° (203), and 32.0° as a contribution from planes (0 0 10) + (1 0 10) were considered.[16,17]

Light Microscopy. Light microscopy investigations were performed for 8 μm thick sections of selected samples. Thin slices were cut in the FD in the plane perpendicular to the constraint direction (CD). The sections were prepared at ambient temperature using a Tesla BS 490A

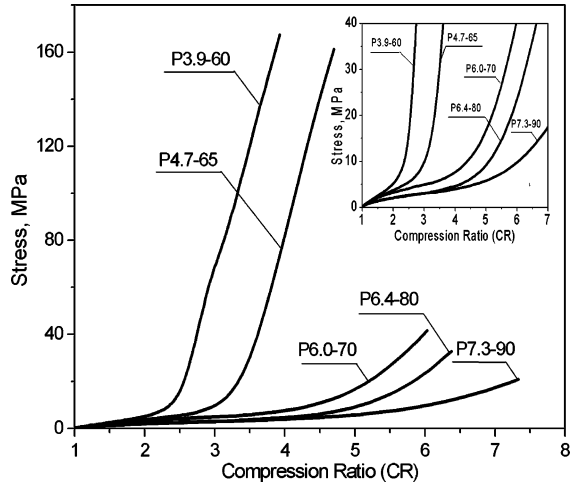

Figure 2. Examples of dependencies of true stress vs compression ratio (CR) recorded for samples deformed in a channel-die at different temperatures at a true strain of 8%/s. Sample codes are given at the curve. The inset illustrates the response at the initial stage of the deformation process.

ultramicrotome equipped with a glass knife. A polarizing microscope with visible light was used (Polish Optical Works, Warsaw).

Mechanical Properties. The mechanical tests were carried out in a tensile mode using an Instron testing machine model 1114 at room temperature. Oar-shaped samples with a gauge length of 9 mm and a width of 2.4 mm were cut out from the oriented material, gauge length parallel to the FD. The samples were tested in the flow (orientation) direction (FD) at the initial deformation rate of 0.5 mm/min. The Young's modulus, the yield stress, and ultimate strength were calculated from the nominal stress versus nominal strain dependencies.

Viscoelastic Properties. Dynamic mechanical properties of selected oriented and unoriented samples were measured using an MkIII DMTA apparatus (Rheometric Scientific, Inc.) in a dual-cantilever bending mode. The oriented samples were deformed periodically in the LD direction. The dynamic storage and loss moduli (E' and E'') were determined at a constant frequency of 1 Hz as a function of temperature from −100 to 145 °C at a heating rate of 3 °C/min.

Results and Discussion

Mechanical Behavior in Compression. Figure 2 shows exemplary stress versus CR dependencies for samples deformed at the same true rate (8%/s) at different temperatures: 60, 65, 70, 80, and 90 °C—samples P3.9−60, P4.7−65, P6.0−70, P6.4−80, and P7.3−90, respectively. The stress is equivalent to the true stress because the sample cross section is constant in a channel-die. The CR can be converted to the true strain e by formula $e = \ln(\mathrm{CR})$.[28]

From Figure 2 it is seen that at the deformation temperatures of 60 and 65 °C, i.e., slightly above T_g, the stress rapidly increases at low CR values of 2.0 and 3.0, respectively. At higher temperature the stress significantly decreases allowing it to reach higher final CR values. However, each curve shows three characteristic regions: the initial low increase of the stress (view the inset in Figure 2), then the plastic flow (plateau) with poor dependency on CR. The plateau is followed by the increase of the load due to strain hardening. The overall response is similar to that observed for other polymers deformed by plane-strain compression above T_g. The dependencies in Figure 2 demonstrate clearly the enhancement of the ability for plastic deformation with the increase of deformation temperature up to 90 °C. For instance, the ultimate compression stress reaches about 160 MPa at 65 °C (at CR = 3.9) and about 20 MPa at 90 °C (at CR = 7.3), respectively. At temperatures higher than 100 °C the polymer flows easily, and no hardening effect is observed.

The increase of CR may lead to a partial disentanglement of the polymer chain often accompanied by mechanical chain scission. A high reduction of molecular weight would not allow the achievement of a high degree of chain orientation and good mechanical performance of the resultant material. Therefore, for selected samples (P4.7−65, P15.7−90, P23.5−90) their molecular weight, M_n, was controlled—the values obtained were, however, close to those for the initial sample (within an experimental accuracy of 10%). For comparison, solid-state extrusion of poly(lactide) through a rectangular die led to a decrease of molecular weight of about 10%.[21]

Structural Alternation. *2D-WAXS Observation*. Structural changes in compressed samples were tested preliminary using the 2D-WAXS method. Figure 3a−f shows 2D-WAXS patterns recorded for the undeformed sample (reference) and samples compressed at different temperatures to CR from 3.9 to 7.3—samples P3.9−60, P4.7−65, P6.0−70, P6.4−80, and P7.3−90, respectively. Figure 3, parts g and h, shows additional 2D-WAXS patterns for samples compressed at 90 °C to higher CR (P15.7−90 and P23.5−90). The patterns are viewed in the LD with the FD directed horizontally.

As expected, for the undeformed sample a diffuse ring characteristic for fully amorphous packing is observed. To our surprise the patterns for samples compressed at the temperatures from 60 to 70 °C (P3.9−60, P4.7−65, P6.0−70) reveal traces of two polar diffraction reflections in the CD direction. These reflections become more intense and confined at higher CR attained at the temperature range from 80 to 90 °C. They are present together with four other weaker reflections appearing at a larger scattering angle 2θ and inclined toward FD at about $\mu \approx 61°$. The changes of the 2D-WAXS images reflect a transition of the initially amorphous structure into an oriented crystalline structure induced by the plane-strain compression at temperatures above T_g. The temperature range of 80−90 °C appeared to be optimal for producing orientation-induced crystallization in the initially amorphous P(L/DL)LA. At higher temperature (100 °C) viscous flow and faster orientation relaxation predominated leading to lower orientation and lower crystallization.

The crystalline structure of the compressed samples was characterized based on X-ray intensity distributions, $I = f(2\theta)$, recorded for the observed reflections. In order to trace different crystallographic planes the investigated sample was scanned in the reflection and transmission modes being faced toward the incident X-ray beam with the loading and flow directions, respectively. Figure 4 shows exemplary diffractograms obtained for the sample P23.5−90, in which the orientation-induced crystallization was most pronounced (Figure 3h). Similar diffractograms were obtained for the sample P15.7−90, while for the sample P4.7−65 only weak diffraction peaks were observed.

The undeformed sample is characterized by a broad diffraction reflection with the maximum around 16.4° (Figure 4, curve 7). Its intensity is higher than the amorphous contribution of the compressed samples. Diffractograms of the deformed sample allow us to assess 2θ positions of the revealed diffraction peaks. The most pronounced one is at 16.8°. Considerably less intense peaks appear at $2\theta = 19.2°$ and 22.2°. They match perfectly to the set of planes (200) or (110), (203), and (015) of the α crystalline form of poly(lactide), respectively.[7,8] We used the

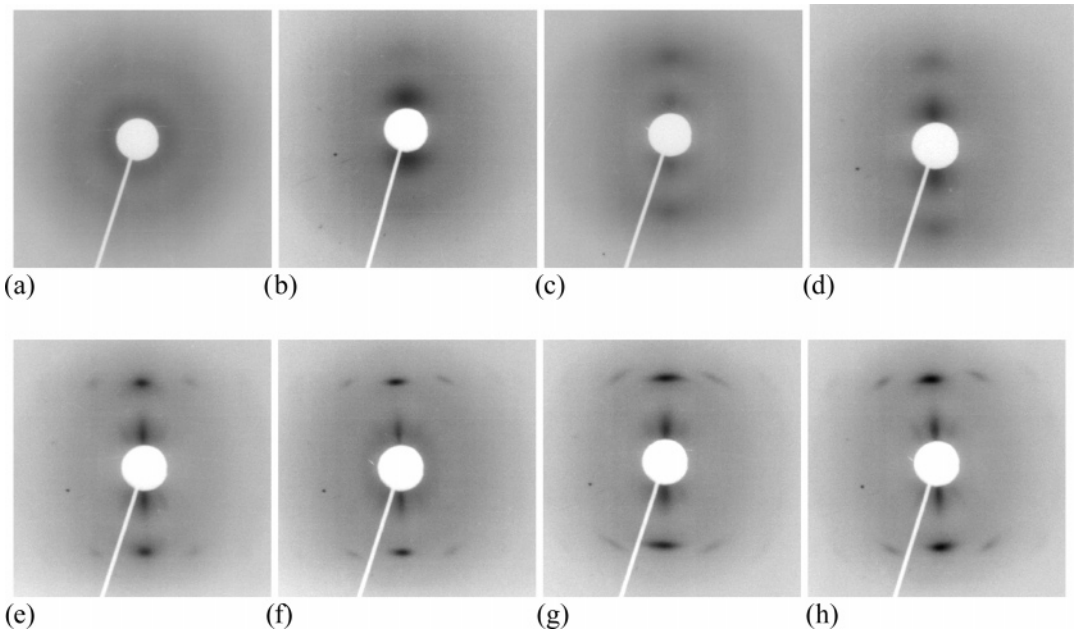

Figure 3. WAXS images of the undeformed sample P1.0 (a) and deformed samples in a channel-die at temperatures from 60 to 90 °C to different compression ratios (CR): P3.9−60 (b), P4.7−65 (c), P6.0−70 (d), P6.4−80 (e), P7.3−90 (f), P15.7−90 (g), and P23.5−90 (h). The patterns are viewed in the load direction (LD) with the flow direction (FD) directed horizontally.

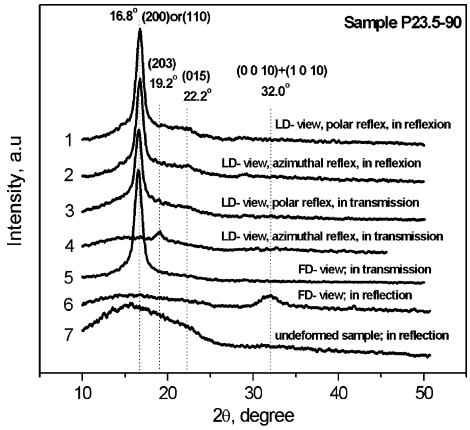

Figure 4. Diffractograms recorded for polar and azimuthal reflections in the transmission and reflection modes for the sample P23.5−90 differently oriented with respect to the incident beam. At each curve the mode and position of the sample with respect to the incident beam are given. For the sample faced with the flow direction (FD view) toward the incident X-ray, the intensity distribution does not change after rotation around the FD when measured in reflection mode (curve 6). For comparison, a diffractogram of the undeformed sample is given (curve 7).

width of the peak at half-maximum at $2\theta = 16.7°$ (planes (200) or (110)) to determine the mean crystallite size (D) in the direction perpendicular to the (200) or (110) planes from the Debye−Scherrer formula[29]

$$D = K\lambda/\mathrm{FW}\cos\theta$$

where K is the shape factor of the average crystallite (assumed here to be 0.9), λ is the wavelength, FW is full width of the considered peak at half-maximum, and θ is its angular position. As the corresponding crystalline planes are parallel to the polymer chain, the D value characterizes the crystallite size in the direction transverse to the chain orientation. The calculations were performed for selected samples P4.6−65, P15.7−90, and P23.5−90. It demonstrates that the increase of the CR from 4.6 to 15.7 leads to crystallites with the size from 18 to 94 Å, respectively. Further increase of the deformation to CR = 23.5 slightly decreases the crystallite width (to 83 Å) in comparison to that of the sample of CR = 15. This thinning of crystalline regions suggests that crystals which were already formed at lower CR undergo an intracrystalline slippage in planes parallel to the chain direction. Deformed samples also reveal the diffraction maximum in the 2θ range from 28° to 36° (see Figure 4, curve 6). This maximum is absent for the amorphous (undeformed) sample. It develops significantly with the increase of CR and is detected only for samples investigated in the reflection mode and faced with the FD toward the incident X-ray beam. As noticed above, the X-ray intensity distribution did not show any changes during rotation of the sample around the FD. This fact suggests a structural symmetry around the FD typical for a fibrous structure with the symmetry axis along the FD. Thus, the crystallite size calculated above can be referred to the width of fibrous crystallites. Evolution of the diffraction maximum at around $2\Theta = 32°$ with increasing CR (samples P4.7−65, P15.7−90, and P23.5−90) is illustrated in Figure 5.One can see that these maxima are composed of at least two overlapping larger diffraction reflections, the relative intensities of which are changing with changing CR. Computer separation (using combined Gaussian and Cauche profiles) allowed us to determine the two main diffraction contributions (component peaks), at $2\theta = 31.25° \pm 0.10°$ and at $2\theta = 32.1° \pm 0.25°$, which correspond to planes (0 0 10) and (1 0 10) of the α form of poly(lactide), respectively. It is seen that the higher the CR the larger the contribution from the (0 0 10) crystalline planes appears.

The evolution of the diffraction peaks at around $2\theta = 32°$ was also observed in the past for semicrystalline poly(lactide) subjected to a solid-state extrusion or tensile drawing to a high ratio.[16,17] In those cases the initial α form was partially transformed to the β form indicated by the appearance of the diffraction peaks of crystalline planes (003) (29.9°) and (023) (31.0°). The ratio of the β to α form was dependent on the deformation conditions (temperature, rate and degree of deformation). Such a transformation process was not detected in any of our samples.

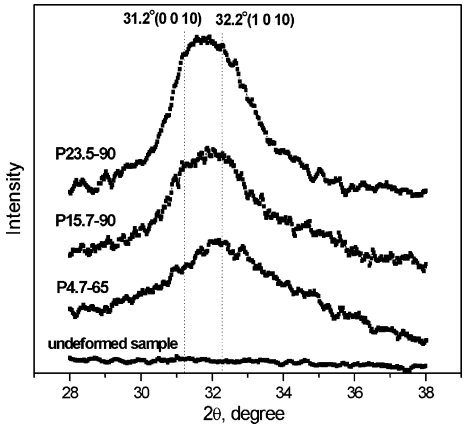

Figure 5. Diffractograms recorded in reflection mode around $2\theta = 32°$ for undeformed and deformed samples with increasing compression ration (CR) (P4.7−65, P15.7−90, and P23.5−90). Deformed samples were faced with the flow direction (FD) toward the incident X-ray beam. The intensity distribution is preserved when the sample was rotated around the axis indicated by the FD. The curves are vertically shifted for clarity.

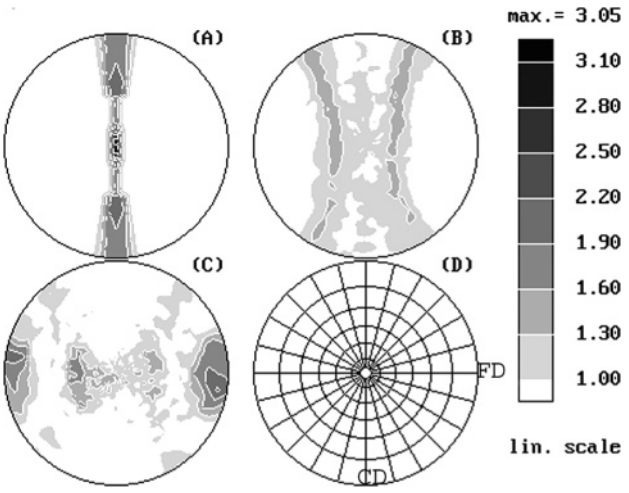

Figure 6. Examples of pole figures of normals to the (200) (A), (203) (B), and both (0 0 10) and (1 0 10) (C) crystalline planes of the α form for the sample compressed in a channel-die to CR = 23.5. All pole figures are viewed in the loading direction (LD), the flow direction (FD) being horizontal; the constraint direction (CD) is vertical (D).

Small-angle X-ray scattering (SAXS) provides information about lamellar organization in a polymer. However, in the case of our channel-die compressed samples no evidence of the periodic packing of lamellar structure was detected. This is because the initial material was amorphous and only extended chain structures were formed as evidenced by the pole figure analysis presented below.

Texture Evolution. The crystalline texture was studied for the P23.5−90 sample, with the most pronounced chain orientation, considering the diffraction peaks at 16.8° (200) and 19.2° (203) as well as the resultant diffraction peak at 32° from the contributions of the (0 0 10) and (1 0 10) crystalline planes (see Figure 4). Exemplary pole figures of normals to the (200), (203), and (0 0 10) + (1 0 10) crystalline planes are shown in Figure 6A−C, respectively. All are viewed in the LD, the FD being horizontal.

The distribution of normals to the (200) crystalline planes shows a well-developed and sharp maximum in the LD and a strong maximum developed in the CD (Figure 6A). The normals to the (203) crystalline planes are inclined to the FD and rotate progressively around the FD (Figure 6B). In the resultant pole figure of the (0 0 10) and (1 0 10) crystalline planes two strong maxima centered around the FD are detected—they originate from (0 0 10) planes and reflect the orientation of the chain axis along the FD (Figure 6C). In this same pole figure also two other weaker maxima around the LD are at the equator. They present the distribution of orientation of normals to the (1 0 10) planes.

The *c*-axis of the unit cell of the α form of poly(lactide) is parallel to the macromolecular chain. The pole figures exhibit uniform arcs crossing the pole figure for the planes containing chain axes; hence, they indicate a well-developed fibrillar texture oriented in the FD. Such an orientation was deduced from the comparison of individual $I = f(2\theta)$ scans recorded for different orientations of the samples. The fibrillar texture was produced in spite of the natural tendency of the plane-strain compression to form a single-crystal-like texture. The fibrillar texture was developed from initially amorphous material; thus, the main transformation mechanism was shear and orientation-induced crystallization. Crystallographic slip simultaneous to transformation processes, at least at the initial stages of deformation, was not detected.

The plane-strain compression-induced structural changes are also accompanied by changes in segmental orientation and consequently by changes in conformational distribution. The phenomena of conformational changes in amorphous PLA during biaxial deformation were investigated in detail elsewhere.[30,31] PLA in cited works contained less D-content; thus, the conformational changes in our case are expected to be different than those in refs 30 and 31. In addition, PLA from refs 30 and 31 had more stereoregular structure and was more prone to strain-induced crystallization than the PLA used in this work.

Morphological Alternations. Polarized light micrographs of thin (8 μm) sections of selected samples, P1.0 (uncompressed), P4.7−65, and P23.5−90, viewed in the CD do not show any features of crystalline regions arranged into supermolecular structures. This indicates that the compressed samples, in spite of orientation and substantial crystallinity, do not have supermolecular structure developed on the level detectable by light microscopy.

TMDSC Characterization. Figure 7a shows an example of the total TMDSC scans for the considered samples. The undeformed sample (P1.0) exhibits only the glass−rubber transition. It is followed by a small endothermic peak related to the segmental relaxation of chains in the amorphous phase connected with aging and usually called "enthalpy relaxation". No cold crystallization and melting processes occurred. The latter was also observed for the P1.0−100 sample which was annealed at 100 °C for 3 h before the scan. This sample exhibited only slightly modified glass transition region due to a different thermal history. With an increase of CR (and deformation temperature) the glass−rubber transition shifts toward higher temperature, and it is followed by an increasing endotherm ascribed to the relaxation of orientation. At higher temperature the melting endotherm appears, the magnitude of which increases with increasing CR up to 7.3. At CR larger than 7.3 the magnitude of this thermal event is not increased noticeably. These observations are consistent with the X-ray data indicating that the crystallite sizes are essentially similar in the samples with CR 7.3 and 23.5. For the sake of analysis the curves of the total heat flow were separated into a reversing signal (the glass transitions, melting) and a nonreversing signal (contains kinetic events such as enthalpy relaxation, cold crystallization, curing, decomposition reactions).[32] An example

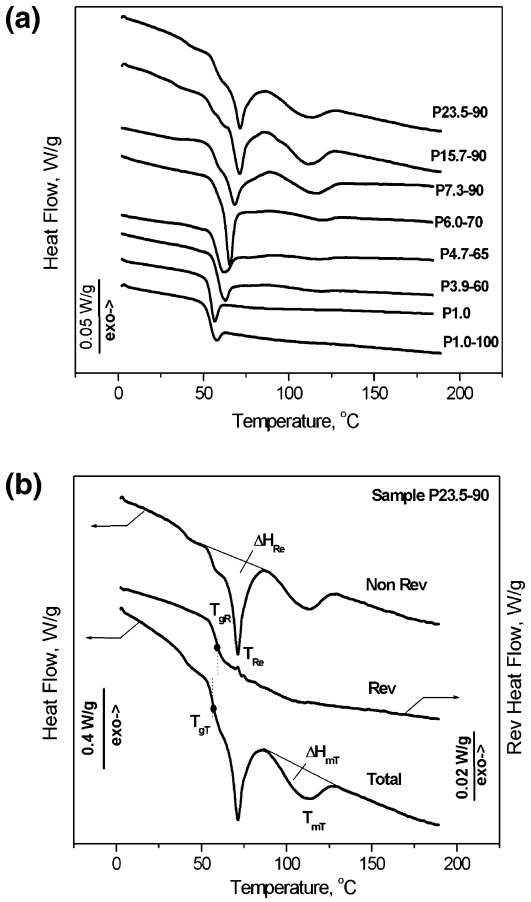

Figure 7. (a) Total TMDSC thermograms for selected samples with increasing compression ratios (CR) (3 °C/min, $A = 0.318$ °C, $P = 40$ s). (b) Example of the separation of total heat flow (Total) on the reversing (Rev) and nonreversing (Non-Rev) signals for sample P23.5−90. Definitions: T_{gT} and T_{gR}, the glass transition temperatures calculated from the total and reversing signals; ΔH_{Re}, T_{Re}, relaxation enthalpy assessed from the relaxation endotherm of the nonreversing signal and the temperature of its maximum; ΔH_{mT}, T_{mT}, the enthalpy of the melting process and its peak temperature determined from the melting endotherm of the total heat flow.

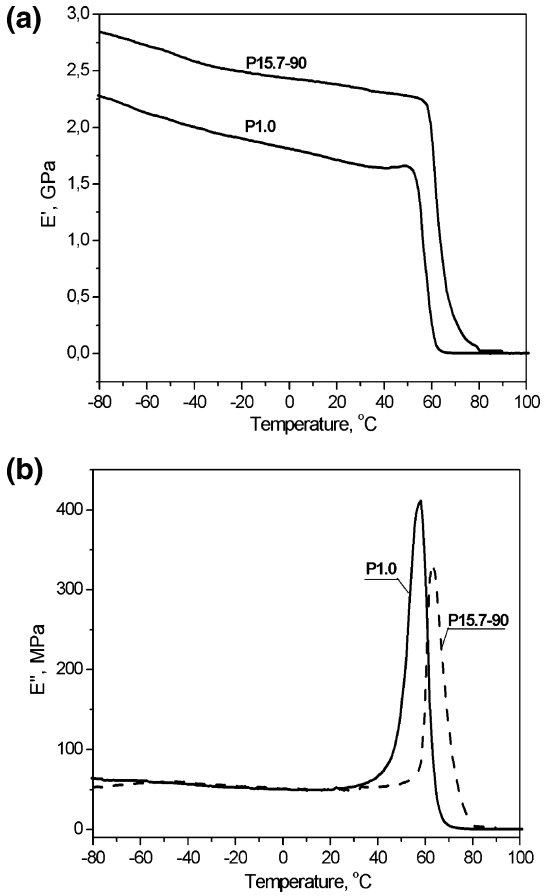

Figure 8. Example of dependencies of the E' (a) and E'' (b) vs temperature for undeformed sample P1.0 and oriented sample P15.7−90 (at 1 Hz, 2 °C/min). The amplitude of the deformation was applied in the loading direction (LD).

of such a separation for sample P23.5−90 is shown in Figure 8b. It is seen that the reversing signal demonstrates an endothermic step change at the glass−rubber transition (T_{gR}) (separated from other effects) and a small melting effect (1.4 J/g) at higher temperature range. The nonreversing signal shows the relaxation endotherm and melting endotherm. The thermal events were quantitatively characterized by the following parameters: T_{gT} and T_{gR}, the glass transition temperatures calculated from the inflection point of the total and reversing signals for comparison; ΔH_{Re}, T_{Re}, the relaxation enthalpy assessed from the relaxation endotherm of the nonreversing signal and the temperature of its maximum; ΔH_{mT}, T_{mT}, the enthalpy of the melting process and its peak temperature determined from the melting endotherm of the total heat flow. These parameters are indicated at the corresponding curves in Figure 7b, and their values are collected in Table 2. It is seen that the T_{gR} is higher than the T_{gT} and both increase with increasing CR.

The increase in T_{gR} is from 57.4 to 60.3 °C for samples P1.0, P3.9−60, P4.7−65, and P6.0−70, and then from 57.8 to 58.9 °C for samples P7.3−90, P15.7−90, and P23.5−90, respectively. The glass−rubber transition is related to the segmental mobility of chains in the amorphous phase. Thus, the increase in the glass−rubber transition temperature with CR reflects an increase of orientation of chains and their constraints related to tighter packing of parallel chains and combined with crystallinity development. The crystallinity degree reaches the highest level for the samples compressed at 90 °C ($X_c = 6.5$−8.9%). It is worth mentioning that initially amorphous poly(L/DL-lactide) of composition 80/20, i.e., more chemically stereoregular than considered in this work, developed 25% crystallinity upon solid-state extrusion.[20]

As seen in Figure 7a, the glass transition is immediately followed by a distinct endotherm which is attributed to the relaxation process of oriented chains. This process is combined with some shrinkage phenomena just activated above the glass transition temperature. The peak temperature of this endotherm (T_{Re}) and its magnitude (ΔH_{Re}) increase clearly with increasing CR from 60.0 to 71 °C and from 5.1 to 10.0 J/g, respectively (Figure 7b, Table 2). This trend is due to the increase of orientation of the amorphous phase and orientation of crystals developed in the samples.

The melting endotherm is broad ($T_m \approx 109$−118 °C) and is observed only for the compressed samples. Its magnitude increases with the CR giving crystallinity from 0.8% to 8.9%, respectively. The crystallinity seems to reach a saturated level at CR above 7.3. The values of T_m and ΔH_m (related to crystallinity) of the considered samples are low in comparison to those for more stereoregular poly(lactide) of composition 96% L-units and 4% D-units crystallized thermally (e.g., ref 33).

It should be emphasized that there is a partial consistence between the WAXS and DSC data because the size determined from the Debye−Scherrer formula is related to the crystallite

Table 2. Calorimetric Parameters Characterizing Thermal Behavior of the Investigated Samples

	glass transition region				melting region		
sample	T_{gT} (°C)	T_{gR} (°C)	T_{Re} (°C)	ΔH_{Re} (J/g)	T_m (°C)	ΔH_{mT} (J/g)	X_c (%)
P1.0	52.9	57.4	56.2	2.00			
P1.0−100	54.2	56.9	56.6	0.60			
P3.9−60	58.3	58.9	60.0	5.1	118.0	1.20	1.3
P4.7−65	57.4	58.5	63.2	5.3	114.0	0.73	0.8
P6.0−70	59.3	60.3	65.2	6.8	118.0	1.40	1.5
P7.3−90	53.2	57.8	68.3	8.93	114.0	6.30	6.8
P15.7−90	54.2	58.9	70.1	10	110.3	8.3	8.9
P23.5−90	56.8	58.7	71.3	8.6	109.9	6.05	6.5

thickness in the direction transverse to the chain's orientation (in planes (200) or (110)), while those resulting from the DSC parameter, T_m, (using the Gibbs−Thompson equation[34]) is related to the length of crystalline stem. In TMDSC it is seen that recrystallization of oriented samples does not take place; however, structural changes are connected with relaxation processes (dependent on CR) at around T_g. At higher temperatures they are dominated by melting. The systems investigated featured oriented structure without evidence of lamellar organization. The crystallites melt in a broad temperature range (from 80 to 120 °C); therefore, the T_m can be determined from the endotherm with only some accuracy. On the contrary, the considered WAXS peaks are well separated from the amorphous contribution, which allows us to determine the width at half-maximum with good accuracy. Nevertheless, the relations between CR and the crystalline sizes from WAXS and DSC are fulfilled for samples compressed to 15.7 and 23.6, but not for the sample with CR = 4.6 probably due to the structural peculiarities indicated above.

Mechanical Properties. *Viscoelastic Properties*. Figure 8, parts a and b, shows the temperature dependencies of the storage and loss moduli, E' and E'', recorded for the undeformed (amorphous) sample (P1.0) and for the exemplary oriented sample with CR = 15.7 (P15.7−90). The periodic deformation amplitude was applied in the LD, i.e., perpendicularly to the orientation direction (FD). The P1.0 amorphous sample shows a gradual decrease of the E' from 2.4 GPa at −100 °C to about 1.7 GPa at 40 °C and then a rapid drop in the glass transition region close to 1 MPa without an increase at higher temperatures usually connected with crystallization. The latter effect actually reflects the lack of cold crystallization as detected by TMDSC. Interestingly, directly before the glass−rubber transition the E' slightly increases (this can be masked in the log scale). Similar behavior of the E' was also observed in some cases for other amorphous PLA samples; however, the explanation was inadequate.[35] According to our observations such a stiffening effect right before reaching T_g in amorphous PLA is affected by the thermo−mechanical history including aging. The E' increase preceding T_g was damped and slightly shifted to a higher temperature for the undeformed sample stored at ambient conditions. Thus, we believe that this stiffening process has the relaxation origin of chain segments, the intensity of which is decreased under the presence of such internal constraints as orientation and development of crystallinity. The corresponding E'' (loss modulus) peak at 57.2 °C indicates the glass transition temperature from the mechanical test (Figure 8b). This value is close to that determined from the reversing signal (T_{gR}) of the TMDSC (Table 2). Oriented P15.7−90 sample featured an increased value of the E' to about 3.0 GPa at −100 °C and to about 2.3 GPa at 40 °C, without a stiffening effect before T_g as observed for the unoriented sample. For the P15.7−90 sample the E' drops due to the glass−rubber transition being at higher temperature than for the undeformed one. Its T_g determined from the E'' peak is 63.1 °C, i.e., higher by ∼5 °C than that determined from the reversing signal presumably due to shrinkage contributions. The shrinkage process is intensified at around 70 °C (region of the T_{Re}, see Table 2); above 70 °C the E' reaches around 20 MPa in the plateau region.

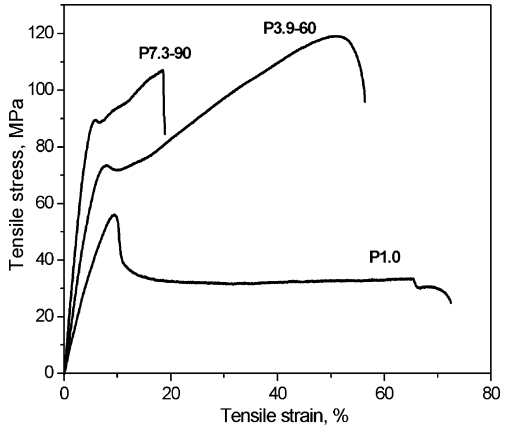

Figure 9. Example of nominal stress vs strain recorded for samples P1.0, P3.9−60, and P7.3−90 at a constant crosshead speed of 0.5 mm/min at ambient temperature. The tensile drawing was conducted along the orientation direction.

Table 3. Tensile Parameters Determined from Nominal Stress−Nominal Strain Curves Recorded for Unoriented Sample P1.0 and Compressed Samples P3.9−60 and P7.3−90, Respectively

sample	initial modulus, E (GPa)	yield stress, σ_y (MPa)	elongation at yield, ϵ_y (%)	ultimate strength, σ_b (MPa)	elongation at break, ϵ_b (%)
P1.0	0.7	55.7	9.6	33.0	65.0
P3.9−60	1.3	73.0	7.5	119.0	51.0
P7.3−90	1.9	89.3	5.8	106.0	18.0

Tensile Properties. Figure 9 shows the nominal stress versus nominal strain dependencies for the unoriented sample, P1.0, and selected samples compressed to different CRs at various temperatures, P3.9−60 and P7.3−90, for comparison. The tensile drawing was conducted along the orientation direction (FD) at a constant strain rate of 0.5 mm/min at ambient temperature.

The tensile properties were characterized by determining the Young's modulus (E), yield stress σ_y with the corresponding elongation at yield ϵ_y, and ultimate stress σ_b with the corresponding elongation ϵ_b. Those parameters are collected in Table 3. Generally, the mechanical performance of the oriented P(L/DL)LA samples increases with the sample orientation. The

modulus increases from 0.7 GPa for the unoriented sample (P1.0) to 1.3 and 1.9 GPa for samples P3.9−60 and P7.3−90, respectively. The yielding region and deformation above it are also influenced strongly by the orientation and crystallization of a sample. For the undeformed sample, a stress after yielding (55.7 GPa, 9.6%) drops to a plateau level (to approximately 33 MPa) which is maintained up to the fracture at an elongation of 65%. In contrast, for the compressed samples P3.9−60 and P7.3−90 the stress after yielding (at 73 MPa, 7.5% and 89.3 MPa, 5.8%, respectively) only slightly drops and then increases to the level of 100−120 MPa with further elongation. The latter effect is due to the strain hardening of the material resulting from the presence of chain entanglements. At the same time the elongation at break is decreased substantially (to 18%) in comparison to that of the undeformed sample (∼70%). Those data show that the mechanical strength of the P(L/DL)LA can be improved substantially by compression-induced orientation and crystallization. It is worth adding that a direct comparison of mechanical data of oriented poly(lactide)s described in the literature can be difficult due to the use of other testing procedures. For example, flexural strength at yield and flexural modulus of solid-state extruded rods of poly(L/DL-lactide) 80/20 reach the level of 177 MPa and 9.5 GPa, respectively.[20]

Conclusion

All deformation processes described in the paper were conducted above the glass transition temperature. Therefore, a substantial molecular rearrangement was possible. To our surprise 70/30 PLA copolymer appears to be crystallizable under the condition of macromolecular orientation imposed by plastic deformation and plastic flow above T_g. Oriented, uniaxially textured poly(L/DL-lactide) samples of low 6−8% crystallinity degree were obtained. The crystalline phase developed was found to be exclusively the α form of poly(lactide). This phase was poorly ordered as indicated by low melting temperature. Neither lamellar nor supermolecular organization was detected as a consequence of the transformation from the initially amorphous, thermally noncrystallizable material. The X-ray reflections from crystallographic planes were rather broad and diffuse suggesting a small size of crystals, much below 100 Å. Such material was characterized by substantially increased mechanical properties: the tensile modulus and ultimate tensile strength increased by 270% and 320−360%, respectively, in comparison with those of the initial amorphous sample. The dynamic storage modulus E', measured in the transverse direction to orientation, increased 135% at 40 °C with respect to that for the starting sample. It is believed that by optimizing the compression conditions the mechanical performance can be further improved, and such investigation are planned to be performed.

Acknowledgment. This work was partially supported by the Ministry of Science and Information Society Technologies (Poland) through the Centre of Molecular and Macromolecular Studies, PAS, under Grant No. PBZ-KBN-070/T09/2001, 2003−2006. The authors gratefully acknowledge the CCA Purac Biochem for supplying P(L/DL)LA.

References and Notes

(1) Kowalski, A.; Duda, A.; Penczek, S. *Macromolecules* **2000**, *33*, 7359−7370.
(2) NatureWorks LLC. Product and Applications. http://www.natureworksllc.com/Product-And-Applications.aspx. (accessed April 5, 2007)
(3) Cicero, J. A.; Dorgan, J. R.; Dec, S. F.; Knauss, D. M. *Polym. Degrad. Stab.* **2002**, *78* (1), 95−105.
(4) Tams, J.; Bos, R. R. M.; Rozema, F. R.; Joziasse, C. A. P.; Grijpma, D. W.; Pennings, A. J. *Biomaterials* **1995**, *16* (18), 1409−1415.
(5) Pennings, J. P.; Dijkstra, H.; Pennings, A. J. *Polymer* **1993**, *34*, 942−951.
(6) Miyajima, M.; Koshika, A.; Okada, J.; Ikeda, M. *J. Controlled Release* **1999**, *60* (2−3), 199−209.
(7) DeSantis, P.; Kovacs, A. J. *Biopolymers* **1968**, *6*, 299−306.
(8) Hoogsteen, W.; Postema, A. R.; Pennings, A. J.; Brinke, G. T.; Zugenmaier, P. *Macromolecules* **1990**, *23*, 634−642.
(9) Kalb, B.; Pennings, A. J. *Polymer* **1980**, *21*, 607−612.
(10) Kobayashi, J.; Asahi, T.; Ichikawa, M.; Okikawa, A.; Suzuki, H.; Watanabe, T.; Fukada, E.; Shikinami, Y. *J. Appl. Phys.* **1995**, *77*, 2957−2973.
(11) Brizzolara, D.; Cantow, H. J.; Diederichs, K.; Keller, E.; Domb, A. J. *Macromolecules* **1996**, *29* (1), 191−197.
(12) Marega, C.; Margio, A.; Noto, V. D.; Zannetti, R. *Makromol. Chem.* **1992**, *193*, 1599−1606.
(13) Miyata, T.; Masuko, T. *Polymer* **1997**, *38* (16), 4003−4009.
(14) Eling, B.; Gogolewski, S.; Pennings, A. J. *Polymer* **1982**, *23* (11), 1587−1593.
(15) Sawai, D.; Takahashi, K.; Imamura, T.; Nakamura, K.; Kanamoto, T.; Hyon, S. H. *J. Polym. Sci., Part B: Polym. Phys.* **2002**, *40* (1), 95−104.
(16) Sawai, D.; Takahashi, K.; Sasashige, A.; Kanamoto, T.; Hyon, S. H. *Macromolecules* **2003**, *36* (10), 3601−3605.
(17) Takahashi, K.; Sawai, D.; Yokoyama, T.; Kanamoto, T.; Hyon, S. H. *Polymer* **2004**, *45* (14), 4969−4976.
(18) Tunc, D. C. *Clin. Mater.* **1991**, *8*, 119.
(19) Törmälä, P.; Rokkanen, P.; Vainionpää, S.; Laiho, J.; Heponen, V. P.; Pahjonen, T. U.S. Patent 4968317, 1990.
(20) Ferguson, S.; Wahl, D.; Gogolewski, S. *J. Biomed. Mater. Res.* **1996**, *30* (4), 543−551.
(21) Lim, J. Y.; Kim, S. H.; Lim, S.; Kim, Y. H. *Macromol. Chem. Phys.* **2001**, No. 11, 2447−2453.
(22) Schmack, G.; Tandler, B.; Vogel, R.; Beyreuther, R.; Jacobsen, S.; Fritz, H. G. *J. Appl. Polym. Sci.* **1999**, *73* (14), 2785−2797.
(23) Cicero, J. A.; Dorgan, J. R. *J. Polym. Environ.* **2001**, *9* (1), 1−10.
(24) Schmack, G.; Tandler, B.; Optiz, G.; Vogel, R.; Kornber, H.; Haussler, L.; Voigt, D.; Weinmann, S.; Heinernann, M.; Fritz, H. G. *J. Appl. Polym. Sci.* **2004**, *91* (2), 800−806.
(25) Okuzaki, H.; Kubota, I.; Kunugi, T. *J. Polym. Sci., Part B: Polym. Phys.* **1999**, *37* (10), 991−996.
(26) Pluta, M.; Bartczak, Z.; Galeski, A. *Polymer* **2000**, *41* (6), 2271−2288.
(27) Fischer, E. W.; Sterzel, H. J.; Wegner, G. *Kolloid Z. Z. Polym.* **1973**, *251*, 980.
(28) Ward, I. M.; Hadley, D. W. *Mechanical Properties of Solid Polymers*; Wiley: New York, 1993.
(29) Alexander, L. E. *X-ray Diffraction Methods in Polymer Science*; Wiley Interscience: New York, 1969; pp 36, 423.
(30) Yang, X. Z.; Kang, S. H.; Yang, Y. N.; Aou, K.; Hsu, S. L. *Polymer* **2004**, *45* (12), 4241−4248.
(31) Tanaka, M.; Young, R. *Biomacromolecules* **2006**, *7* (9), 2575−2582.
(32) TA Instruments. Thermal Analysis and Rheology: Thermal Applications Note, Choosing Conditions in Modulated DSC; TN-45B. http://www.tainstruments.co.jp/application/pdf/Thermal_Library/Applications_Notes/TN045.PDF (accessed April 5, 2007).
(33) Pluta, M.; Galeski, A. *J. Appl. Polym. Sci.* **2002**, *86* (6), 1386−1395.
(34) Hoffman J. D. *Polymer* **1983**, *24* (1), 3−26.
(35) Ouchi, T.; Kontani, T.; Ohya, Y. *Polymer* **2003**, *44* (14), 3927−3933.

BM061229V